Processing and Application of Ceramics 18 [3] (2024) 395–404
https://doi.org/10.2298/PAC2404395Y

Anti-thermal-quenching and colour-tuneable Tb^{3+}/Ce^{3+}-doped phosphor from natural wollastonite

Xinhong Yu, Feng Chen*, Ming Yang, Min Ruan, Wei Feng

Institute of Materials Science and Engineering, Hubei Polytechnic University, Huangshi, 435000, China

Received 5 September 2024; Received in revised form 27 November 2024; Accepted 7 December 2024

Abstract

Series of doped natural wollastonite phosphors (xTb^{3+}/xLi^{+}, yCe^{3+}/yLi^{+} and $xTb^{3+}/0.06Ce^{3+}/xLi^{+}$ co-doped wollastonite) were synthesized by high temperature solid state thermal diffusion method in vacuum furnace. The powders mainly consisted of low temperature α-$CaSiO_3$ phase corresponding to the triclinic crystal structure, and according to ionic radii differences it was proposed that Tb^{3+} and Ce^{3+} had tendency to be incorporated at the Ca^{2+} position. The natural wollastonite powder has primarily needle-like particles with small amount of finer spherical aggregates, whereas the portion of finer particles increases significantly after the doping with Tb^{3+}/Ce^{3+} ions. Under 352 nm light excitation, the Tb^{3+}/Li^{+} co-doped wollastonite phosphors with Tb^{3+}/Li^{+} content between x = 0.08–0.18 achieved tuneable luminescence from green to yellow through energy transfer from Tb^{3+} to minor impurity Mn^{2+} existing in the matrix. All of the Ce^{3+}/Li^{+} co-doped wollastonite phosphors with Ce^{3+}/Li^{+} content between y = 0.02–0.10 emitted intense purple-blue light centred at 382 nm. In the $xTb^{3+}/0.06Ce^{3+}/xLi^{+}$ ($0.01 \leq x \leq 0.09$) co-doped wollastonite phosphors, Ce^{3+} acted as a sensitizer and the energy transfer efficiency from Ce^{3+} to Tb^{3+} reached 62.5%. Temperature dependent photoluminescence within 298–498 K suggested an excellent thermal stability of the $0.06Ce^{3+}/0.06Li^{+}$ co-doped wollastonite phosphor, of which the intensity at 498 K retained 96.2% of that at room temperature. Importantly, anti-thermal-quenching phenomenon was observed in the $0.12Tb^{3+}/0.12Li^{+}$ co-doped wollastonite phosphor, and the 545 nm emission intensity at 498 K reached 120.3% of that at 298 K. The regulation of thermal luminescence behaviour for Tb^{3+} was achieved by incorporating Ce^{3+} ions in the $0.12Tb^{3+}/0.12Li^{+}$ co-doped wollastonite phosphor. Based on the observations, the above materials display good thermal stability and can be developed as phosphors for application in display devices and LEDs above room temperature.

Keywords: *Tb^{3+}/Ce^{3+}-doped wollastonite, optical properties, energy transfer, thermal stability*

I. Introduction

White light-emitting diodes (W-LEDs) are attracting huge attention as a promising solid-state illumination in human daily life owing to their high efficiency, low power consumption, long life time and environment friendly characteristics [1–3]. In commercial W-LEDs, white-light emitting is mostly achieved by the combination of a blue LED chip and yellow-emitting YAG:Ce^{3+} phosphor [4]. Nonetheless, the result is not satisfactory for general lighting, owing to the lack of red components, which leads to a low CRI value (<80) and high CCT (>4000 K) of W-LEDs [5]. To overcome the deficiency, red components are added to the devices via the combination of blue GaN-based chip with the mixtures of green/yellow and red phosphors [6]. An alternative approach to achieve high-quality full spectrum lighting is to match a near-ultraviolet (NUV, 360–420 nm) chip with tricolour (blue + green + red) phosphors. Based on this method, W-LEDs can have excellent spectral continuity which is close to sunlight spectrum [7]. However, this strategy requires high luminescent efficiency of each component phosphor and especially superior thermal stability under NUV light excitation. Presently, tricolour phosphors with strong absorption at NUV light, high emission efficiency and high thermal stability are still lacking.

Among the large number of luminescent hosts, silicates are preferred for research due to their excel-

*Corresponding authors: tel: +8607146358328,
e-mail: *fengfeng198609@sina.com*

lent chemical and thermal stability. Many phosphors based on silicate host have been developed, including $Li_2SrSiO_4:Eu^{2+}$, $KAlSiO_4:Sm^{3+}$, $Ba_2SiO_4:Eu^{2+}$, $Y_2Si_2O_7@Zn_2SiO_4:(Ce^{3+},Mn^{2+},Eu^{3+})$ etc. [8–11]. Except for the above silicate matrices, wollastonite (with theoretical composition of 51.75 wt.% SiO_2 and 48.25 wt.% CaO) has also been reported as phosphor host, which is a polymorphic mineral with a chemical formula of $CaSiO_3$ [12]. The luminescence of α-$CaSiO_3:Eu^{2+}$ was studied by Poort *et al.* [13] which gave poor luminescence at room temperature. Kshetri *et al.* [14] fabricated Yb/Er-doped $CaSiO_3$ β-wollastonite up-conversion ceramic phosphor through microwave hydrothermal method followed up by heat-treatment in air environment. Ma *et al.* [15] synthesized Eu^{2+} doped pseudo-wollastonite α-$CaSiO_3$ blue phosphor, and found that the phosphor shows outstanding temperature stability, which maintains 94.65% of its initial emission intensity at 423 K. However, the researches mentioned above are all carried out based on phosphors with synthetic wollastonite, which can be obtained with high purity.

Naturally occurring wollastonite with high purity can also be used as phosphor host, which has two different structures including α-$CaSiO_3$ and β-$CaSiO_3$ [16]. Among the different types of wollastonite, the most common one in the nature is 1Tr α-$CaSiO_3$, the structure which consists of two layers of [SiO_4] tetrahedral chains and one layer of [CaO_8] chains alternately packed. Calcium ions occupy seven different crystallographic sites which are all coordinated by eight oxygen ions; the crystal structure is plotted in Fig. 1 [17]. Because the crystal structure has multiple ion substitution sites, its properties can be modified by adjusting the doping ions. In our previous work, Eu^{3+} doped natural wollastonite (α-$CaSiO_3$) phosphor with red emission was fabricated successfully and different amount of La^{3+} ions were introduced to redistribute Eu^{3+}/Eu^{2+} activator and regulate the emission colour [18]. However, the corresponding green and blue phosphors based on natural wollastonite have not been reported in detail.

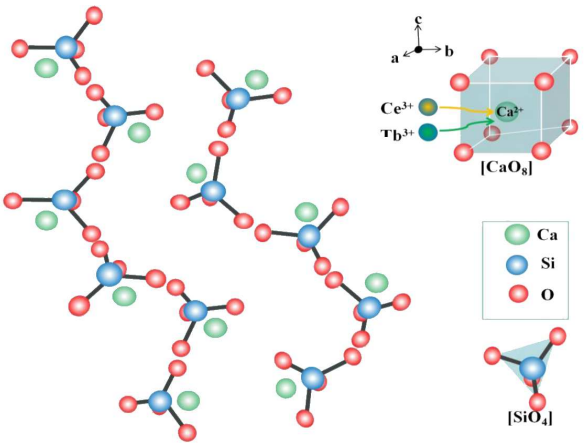

Figure 1. Sketch of the crystal structure of wollastonite (α-$CaSiO_3$) [17]

Among the rare earth ions, Tb^{3+} ($^5D_4$-^7F_J) ion can emit bright green light and is rarely sensitive to the surrounding environment. Ce^{3+} exhibits strong absorption in the ultraviolet region and emits blue to yellow light due to the spin-allowed $4f$–$5d$ energy level transition. Moreover, it can transfer the absorbed excitation energy to other activators to increase the emission intensity. Therefore, the co-doped Ce^{3+} is usually chosen to sensitize Tb^{3+} in order to obtain improved emission [19,20]. Hence, in the present study, to further enrich and improve the luminescence characteristics of natural wollastonite mineral based phosphors, rare earth Tb^{3+}-Ce^{3+} ion pairs were doped into the natural wollastonite matrix. The impact of doped ions on the structure, morphology, photoluminescence properties and thermal stability characteristics of the prepared phosphors were studied in detail. Furthermore, the mechanism and efficiency of energy transfers between Ce^{3+}-Tb^{3+} were also discussed in detail.

II. Experimental

Series of Tb^{3+}/Ce^{3+} co-doped natural wollastonites were synthesized and Li^+ was also added for the charge and size compensation. For the synthesis of Tb^{3+}/Li^+, Ce^{3+}/Li^+ and $Tb^{3+}/Ce^{3+}/Li^+$ co-doped wollastonite phosphors (Table 1) high temperature solid state thermal diffusion method was used. Precursor wollastonite powder was obtained from the quarry in Huangshi, China and has the following composition (according to XRF analyses): 47.85 wt.% CaO, 51.24 wt.% SiO_2, 0.15 wt.% Al_2O_3, 0.15 wt.% MgO, 0.03 wt.% NaO, 0.45 wt.% Fe_2O_3, 0.06 wt.% MnO, 0.04 wt.% SrO and 0.03 wt.% CuO. Natural wollastonite mineral has purple luminescence (under 254 nm lamp excitation) originating from a small portion of Mn^{2+} activator from the natural mineral [21]. Broken pieces of the natural wollastonite were firstly powdered to a uniform consistency (200 meshes) using an agate mortar. High purity rare earth materials Tb_4O_7, CeO_2 (purity >99.99%, Baotou Rare-Earth Institute, PR China) and Li_2CO_3 (A.R) were stoichiometrically weighed according to the desired sample compositions: i) xTb^{3+}/xLi^+ (x is the molar ratio of cations, $n_{Tb^{3+}}/n_{Ca^{2+}}$), ii) yCe^{3+}/yLi^+ (y is the molar ratio of cations, $n_{Ce^{3+}}/n_{Ca^{2+}}$) and iii) $xTb^{3+}/0.06Ce^{3+}/xLi^+$ co-doped natural wollastonite (Table 1). The prepared powder mixtures were then uniformly mixed with the wollastonite powders by ball-milling for 4 h in ethanol. Afterwards, the obtained slurry was dried in an electric vacuum drying oven. Finally, the mixed powder samples in corundum crucibles were heated in vacuum furnace. After heat-treatment at 1150 °C for 2 h, all mixtures were collected after natural cooling to room temperature, and pulverized for further measurements.

X-ray powder diffraction patterns of the products were recorded on a Rigaku D/max-IIIA diffractometer with Cu Kα radiation (λ = 1.5403 Å) at a scanning rate of 8 °/min at 40 kV and 30 mA. X-ray photoelec-

tron spectroscopy (XPS) analyses were conducted on a Thermo Scientific K-Alpha spectrometer. The morphology of the phosphors was observed by scanning electron microscopy (SEM, JSM-6360LV, JEOL, Tokyo, Japan). Photoluminescent excitation and emission spectra were recorded on F-4500 spectrometer with 450 W xenon lamp as the excitation source. The colour coordinates of the samples were calculated by the CIE software. The temperature-dependent emission spectra from 298 to 498 K were measured by a high-temperature heating stage with mode of TAP-02 (Tian Jing Orient-KOJI instrument Co. Ltd.). Except for the temperature-dependent photoluminescent test, all the measurements were performed at room temperature.

Table 1. Sample notation of different wollastonite based phosphors

Sample notation	Doping content	
	Tb^{3+}/Ca^{2+} (x)	Ce^{3+}/Ca^{2+} (y)
Wo-Tb-0.01	0.01	
Wo-Tb-0.03	0.03	
Wo-Tb-0.09	0.09	
Wo-Tb-0.12	0.12	
Wo-Tb-0.15	0.15	
Wo-Tb-0.18	0.18	
Wo-Ce-0.02		0.02
Wo-Ce-0.04		0.04
Wo-Ce-0.06		0.06
Wo-Ce-0.08		0.08
Wo-Ce-0.10		0.10
Wo-Ce/Tb-0.01	0.01	0.06
Wo-Ce/Tb-0.03	0.03	0.06
Wo-Ce/Tb-0.05	0.05	0.06
Wo-Ce/Tb-0.07	0.07	0.06
Wo-Ce/Tb-0.09	0.09	0.06

III. Results and discussion

3.1. Phase composition and crystal structure

XRD patterns of the xTb^{3+}/xLi^{+} ($0 \le x \le 0.15$), yCe^{3+}/yLi^{+} ($0 \le y \le 0.10$) and xTb^{3+}/0.06Ce^{3+}/xLi^{+} ($0 \le x \le 0.09$) co-doped wollastonite phosphors are shown in Figs. 2a, 2b and 2c, respectively. The XRD pattern of the undoped natural wollastonite is also measured for comparison, which mainly consists of low temperature α-$CaSiO_3$ phase, corresponding to the triclinic crystal structure with space group $P\bar{1}$ (PDF 27-1064) [22]. Considering that the radii of Tb^{3+} (r = 1.04 Å, CN = 8) and Ce^{3+} (r = 1.14 Å, CN = 8) are similar to those of Ca^{2+} (r = 1.12 Å, CN = 8), it is deduced that Tb^{3+} and Ce^{3+} tend to be incorporated into the Ca^{2+} position. The introduction of radius percentage difference (D_r) provides a theoretical basis for the ion substitution inference and can be calculated by the following equation:

$$D_r = \frac{R_m(CN) - R_d(CN)}{R_m(CN)} \quad (1)$$

where $R_m(CN)$ and $R_d(CN)$ are radii of the substituted and original ions in the matrix (for the corresponding coordination number, CN), respectively. The calculated D_r values for Ca^{2+}/Tb^{3+} and Ca^{2+}/Ce^{3+} are 7.69% and 1.75%, respectively, both below 30%, suggesting that Tb^{3+} and Ce^{3+} can easily replace Ca^{2+} in the wollastonite matrix.

After the doping with Tb^{3+}/Ce^{3+} and Li^{+} ions, both the broadening of diffraction peaks and the reduction of intensity are observed. The phenomenon may be

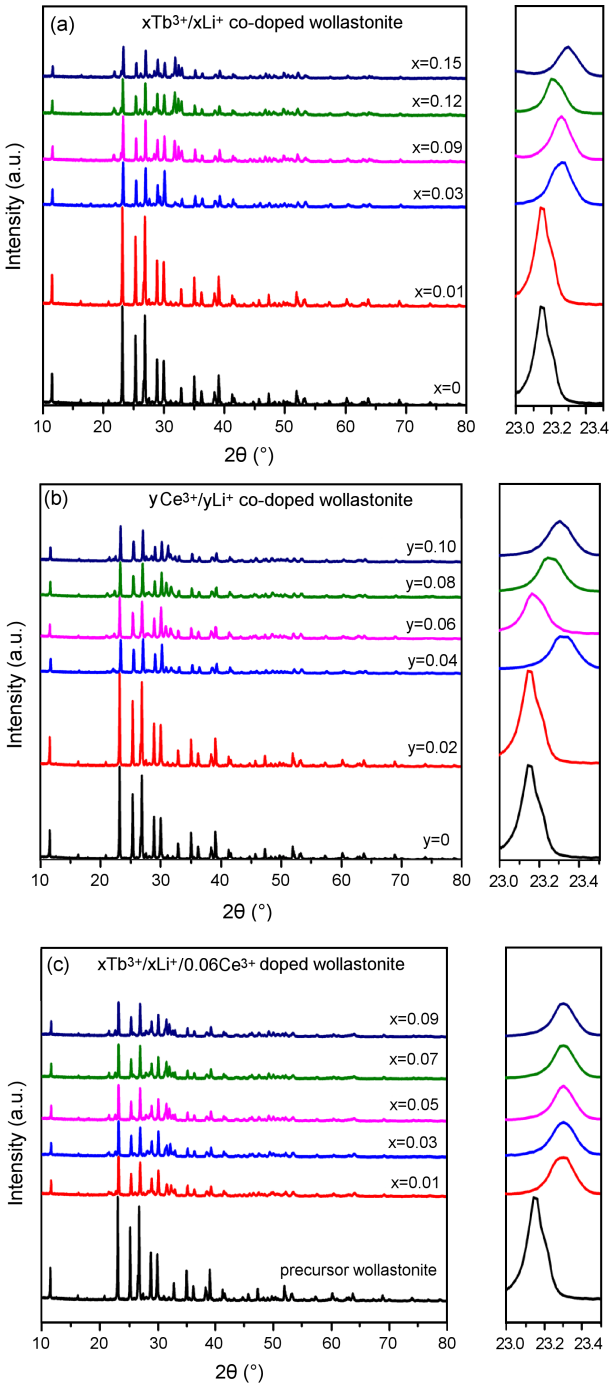

Figure 2. X-ray diffraction patterns of wollastonite based phosphors: a) xTb^{3+}/xLi^{+} ($0 \le x \le 0.15$), b) yCe^{3+}/yLi^{+} ($0 \le y \le 0.10$) and c) xTb^{3+}/0.06Ce^{3+}/xLi^{+} ($0 \le x \le 0.09$)

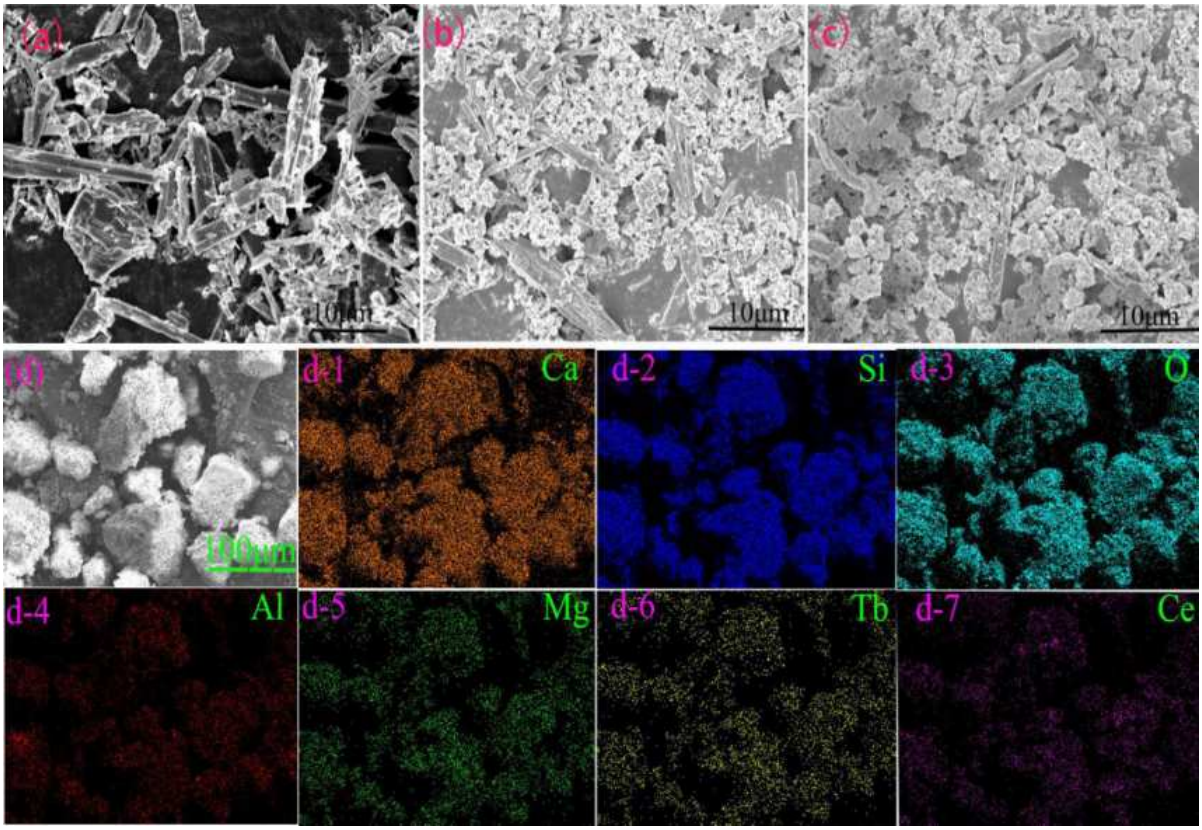

Figure 3. SEM images of natural wollastonite (a) 0.12Tb^{3+}/0.12Li^{+} co-doped (b) and 0.06Ce^{3+}/0.06Li^{+} co-doped samples (c), as well as EDS mapping of Ca, Si, O, Al, Mg, Tb and Ce in 0.12Tb^{3+}/0.06Ce^{3+}/0.12Li^{+} co-doped wollastonite sample (d1-d7)

caused by the infiltration of the doped ions which can degrade the crystallinity of the wollastonite mineral. Although there is no detectable impurity peaks, the diffraction peaks obviously shift towards higher diffraction angles (Fig. 2). In the case of Tb^{3+}/Li^{+} co-doped wollastonite phosphors with Tb^{3+}/Li^{+} content $0 \leq x \leq 0.15$, both radii of Tb^{3+} and Li^{+} are smaller than that of Ca^{2+} ions, which results in lattice contraction according to the Bragg formula $2d \sin\theta = n\lambda$ [23]. Thus, higher doping concentration of smaller ions resulted in more significant shifts toward higher diffraction angles. For the Ce^{3+}/Li^{+} co-doped wollastonite phosphors with Ce^{3+}/Li^{+} content $0 \leq y \leq 0.10$, where Ce^{3+} ions are slightly larger than Ca^{2+} ions and with presence of much smaller Li^{+} ions, lattice shrinks and the corresponding displacement of crystalline diffraction peaks are also observed (Fig. 2).

3.2. Microstructure characterization

The representative natural wollastonite matrix and the co-doped wollastonite phosphors were characterized by SEM technique. It can be seen from Fig. 3a that the natural wollastonite powder has both needle-like microrods and some finer aggregated particles. The coarse microrods exhibit diameter around 10 μm and several tens of micrometers in length, and the grain size of finer particles is between a few microns and dozens of microns. From Figs. 3b and 3c it is clear that the proportion of finer particles increases significantly after the introduction of Tb^{3+}/Ce^{3+} in wollastonite structure. The finer particles may be caused by the generation of fragments during ball-milling process. On the other hand, the infiltration of Tb^{3+}/Ce^{3+} ions into wollastonite matrix could also broke the needle-like microrods into finer pieces. This is consistent with the decreasing and broadening of XRD peaks (Fig. 2), which means the decreasing of mineral crystallinity and crystallite size. To study the distribution of the doped Tb^{3+}/Ce^{3+} ions in the microsphere, the EDS mappings of elements are given in Fig. 3d. It can be seen that the product has seven elements, namely Ca, Si, O, Al, Mg, Tb and Ce, which are evenly distributed in the sample.

3.3. Optical properties - Tb^{3+}/Li^{+}, Ce^{3+}/Li^{+} samples

Figure 4 shows excitation and emission spectra of the Tb^{3+}/Li^{+} and Ce^{3+}/Li^{+} co-doped phosphors. The excitation spectrum (Fig. 4a) of the 0.06Ce^{3+}/0.06Li^{+} co-doped wollastonite phosphor was monitored at 420 nm. A broad excitation band ranging from 200 nm to 400 nm with intense peaks at 254, 284 and 352 nm is observed, which is due to the $5d \rightarrow 4f$ transition of Ce^{3+} ion [24]. The emission spectrum in range from 340 to 500 nm, obtained under 352 nm excitation, is shown in Fig, 4 and has a band centred at 382 nm. Ce^{3+} has an electron configuration of $[Xe]4f^{8}$ and its orbital energy can be divided as ground energy levels of $^{7}F_{j}$ (j = 1–6) and excited levels of $^{5}D_{3}$ and $^{5}D_{4}$.

The excitation spectrum (Fig. 4c) of the

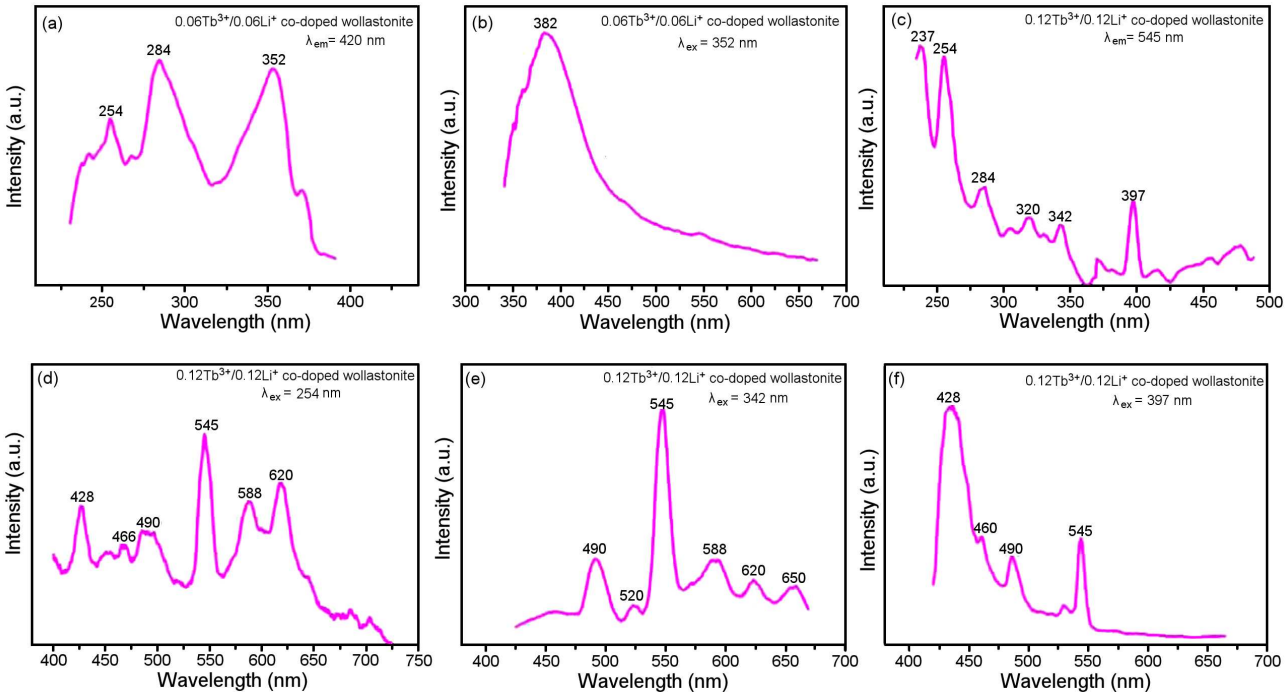

Figure 4. Excitation (a) and emission (b) spectra of 0.06Ce^{3+}/0.06Li^{+} co-doped wollastonite phosphor. Excitation (c) and emission (d-f) spectra of 0.12Tb^{3+}/0.12Li^{+} co-doped wollastonite phosphor under different monitor wavelength

0.12Tb^{3+}/0.12Li^{+} co-doped wollastonite phosphor monitored at 545 nm displays strong excitation in 200–270 nm range peaked at 237 and 254 nm, corresponding to the spin allowable 4*f*–5*d* absorption of Tb^{3+}. The remaining peaks at 320, 342, 370 and 397 nm should be assigned to the intra-4f^8 transitions of $^7F_6$-$^5D_0$, $^7F_6$-$^5G_2$, $^7F_6$-$^5G_6$ and $^7F_6$-$^5D_2$, respectively [25].

A comparison of luminescence character of the 0.12Tb^{3+}/0.12Li^{+} co-doped wollastonite phosphor under 254, 342 and 397 nm excitation wavelengths is shown in Figs. 4d-f, respectively. As it can be seen, the sample exhibits two sets of emission bands under 254 nm excitation. The emission peaks at 490, 545, 588 and 620 nm are ascribed to the $^5D_4$-^7F_J (J = 6, 5, 4, 3) transitions, while the emission peaks at 428, 455 and 466 nm are attributed to the $^5D_3$-^7F_J (J = 5, 4, 3) transitions of Tb^{3+} ions [26]. Different from the emission of Tb^{3+} in other phosphors based on synthetic matrix, the 588 and 620 nm peaks in present work are both relatively high, the intensity of which reach almost that of the main peak at 545 nm. In the case of 342 nm excitation, the $^5D_3$-^7F_J (J = 5, 4, 3) transitions of Tb^{3+} are not observed. Noteworthy is that despite of the $^5D_4$-^7F_J (J = 6, 5, 4, 3) transitions at 490, 545, 588 and 620 nm, two minor emission peaks at 520 and 650 nm appear, which are usually reported as the emission of Eu^{3+} emission centres. Though the elements present in the wollastonite matrix confirmed that the raw materials used in this study naturally exist in low-grade impurity contents, the spectra difference may be caused by the minor amount of impurity ions. Under 397 nm excitation (Fig. 4f), the emission spectrum is consisted of both the strong $^5D_3$-^7F_J emission band located at 428 nm and the $^5D_4$-^7F_J peaks at 490 and 545 nm. In addition, one should notice that the intensity of $^5D_3$-^7F_J transition is much stronger than that of the $^5D_4$-^7F_J transition. The

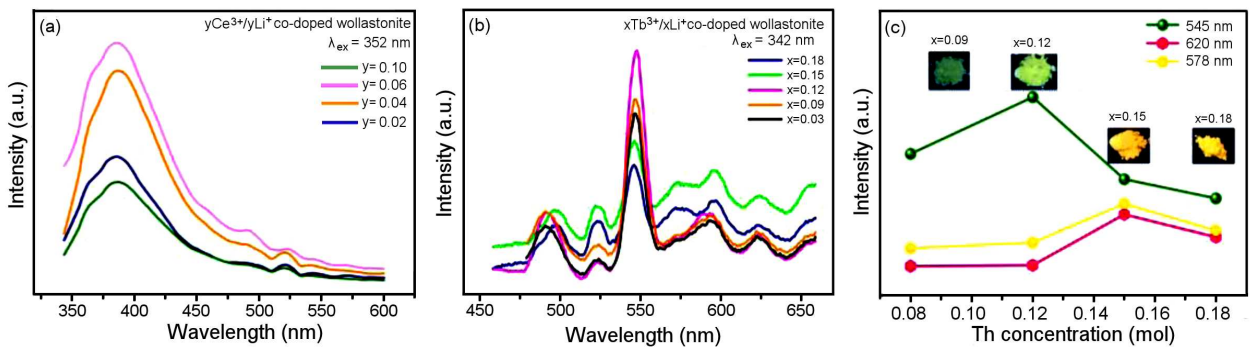

Figure 5. Emission spectra of *y*Ce^{3+}/*y*Li^{+} co-doped (a) and *x*Tb^{3+}/*x*Li^{+} co-doped wollastonite phosphors (b) as well as concentration-dependent intensity of 545, 578 and 620 nm emission peaks of Tb^{3+} ions (c)

above findings imply that the Ce^{3+}/Tb^{3+} doped phosphors can be properly excited by a UV/near-UV LED chip. Besides, 254 and 342 nm excitations are effective for $^5D_4$-^7F_J (J = 6, 5) transitions, while the 397 nm UV light is more efficient for the $^5D_3$-^7F_J transitions of Tb^{3+} ions.

The luminescence property of a phosphor depends on the concentration of doped ions inside it. It can be clearly observed from Fig. 5a that the variation of Ce^{3+} concentration causes variation in the emission intensities, but the profile of the spectra remains invariant. As the doping concentration of Ce^{3+} ions increases from 0.02 to 0.06, the emission intensity enhances and it becomes optimal at y = 0.06. Further increase in the doping value from 0.06 to 0.10 reduces the emission intensity because of the concentration quenching effect. In case of the xTb^{3+}/xLi$^+$ co-doped wollastonite phosphors, when Tb^{3+} doping concentration increases from 0.03 to 0.12, the intensity enhances but the spectra shapes remain the same (Fig. 5b). However, with further increase of x value above 0.12, the peak at 545 nm decreases, while the peak at 578 nm appears and increases gradually. The emission intensities of 545, 578 and 620 nm peaks are plotted versus the Tb^{3+} concentration, which are shown in Fig. 5c. It is obvious that the G/Y (green to yellow) ratio continuously decreases, resulting in the change of emission colour from green to yellow. The corresponding digital photos under 365 nm lamp are also given in Fig. 5c and it can be seen clearly that the colour change from blue-green to yellow with the increase of Tb^{3+} ions. Generally, the $^5D_4 \rightarrow {}^7F_4$ and $^5D_4 \rightarrow {}^7F_3$ transitions of Tb^{3+} at 586 and 620 nm are very weak. Presently, the ratio of 586 and 620 nm band intensities to the intensity of 545 nm band is relatively high in the natural xTb^{3+}/xLi$^+$ co-doped wollastonite phosphors. Besides, the 578 nm yellow emission band is usually reported as $^4T_1$-$^6A_1$ spin flip transition within the d-electrons of Mn^{2+} ion. Thus, it can be concluded that natural wollastonite does contain trace amounts of Mn element, which cannot emit strong light due to lower content or uneven distribution. However, in the sample with higher Tb^{3+} concentration, the energy transfer process between $Tb^{3+} \rightarrow Mn^{2+}$ happens simultaneously, resulting in the appearance of 578 nm emission and the superposition of emission spectra between Tb^{3+} and Mn^{2+} in the range of 580–650 nm. Similar phenomenon ($Tb^{3+} \rightarrow Eu^{3+}$) has also been reported by Halmurat *et al.* [27] in Tb^{3+} doped natural sodium feldspar.

3.4. *Optical properties - $Tb^{3+}/Ce^{3+}/Li^+$ samples*

Figure 6a shows the excitation spectrum of the Tb^{3+}/0.06Ce^{3+}/Li^+ co-doped wollastonite phosphors with Tb^{3+}/Li^+ content x = 0.01, 0.03, 0.05, 0.07 and

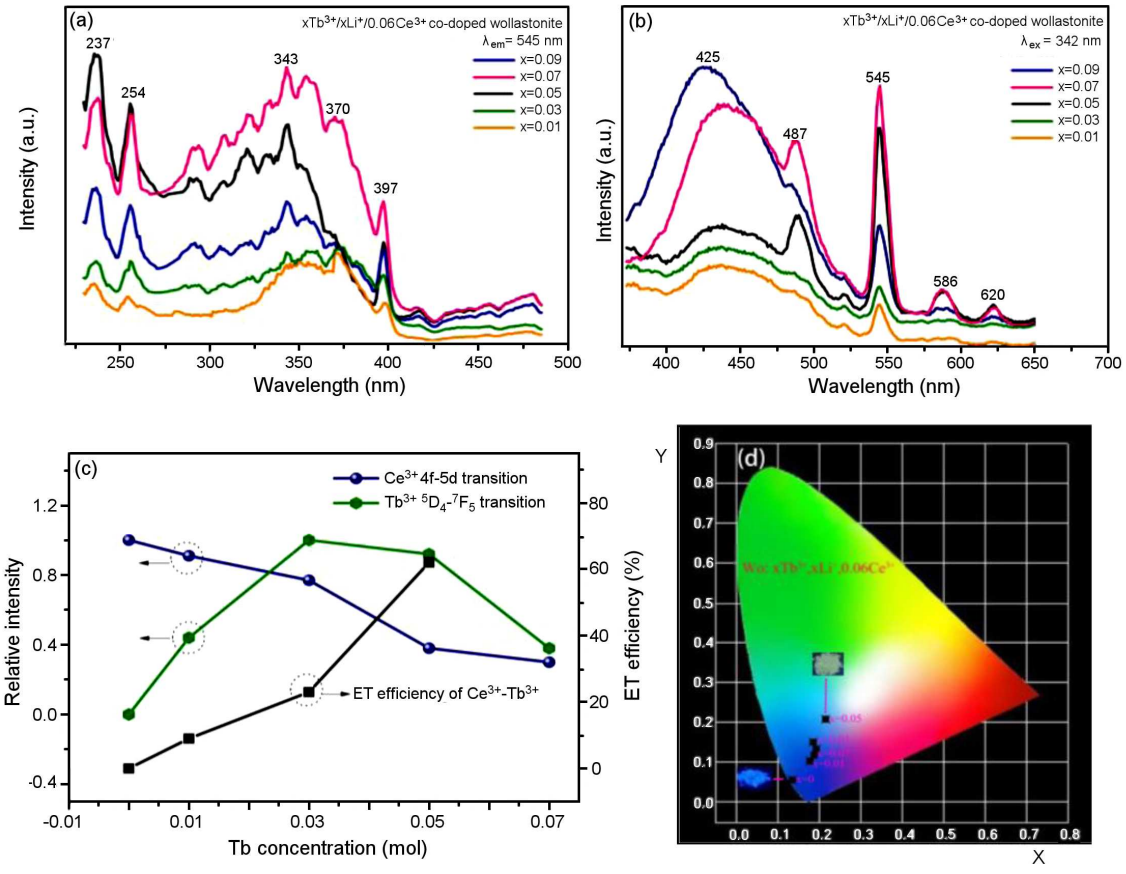

Figure 6. Excitation (a) and emission spectra (b) dependence of Ce^{3+} emission, Tb^{3+} emission and energy transfer efficiency on Tb^{3+} concentration (c) and CIE chromaticity coordinates (d) of xTb^{3+}/0.06Ce^{3+}/xLi$^+$ phosphors

0.09 monitored at 545 nm. Despite the intense excitation peaks at 237 and 254 nm in O^{2-}-Tb^{3+} charge transfer zone, this excitation spectrum includes the broad band of Ce^{3+} between 300–400 nm and the sharp peaks of Tb^{3+} at 342, 370 and 397 nm. Therefore, there is a superposition of excitation spectra between Ce^{3+} and Tb^{3+} in the range of 300–400 nm. Figure 6b demonstrates the emission spectra of the $Tb^{3+}/0.06Ce^{3+}/Li^{+}$ co-doped wollastonite phosphors with Tb^{3+}/Li^{+} content $x = 0.01, 0.03, 0.05, 0.07$ and 0.09 on 342 nm excitation. Noteworthy is that in the $Tb^{3+}/0.06Ce^{3+}/Li^{+}$ co-doped phosphor, the 578, 586 and 626 nm emission peaks are relatively weak compared to the Tb^{3+}/Li^{+} doped sample. The energy transfer process between $Tb^{3+} \rightarrow Mn^{2+}$ may be interrupted by Ce^{3+} ions to a certain extent. Besides, we can find that the emission peak of Ce^{3+} shifts from 382 to 425–430 nm. Simultaneously, the intensity of Ce^{3+} decreases and the Tb^{3+} ions increases gradually with the increasing of Tb^{3+} from $x = 0.01$ to 0.05, indicating that the energy of Ce^{3+} is transferred to Tb^{3+} ions, as reported in many references. Thus, Ce^{3+} can have a key role in the Tb^{3+} luminescence sensitization due to the *f-d* transition. However, when the Tb^{3+} concentration is higher ($x > 0.05$), both Ce^{3+} and Tb^{3+} emission intensity decrease significantly, which may be caused by the concentration quenching effect.

The energy transfer efficiency (η_T) is calculated based on the variation of emission intensity of Ce^{3+} by the following equation [28]:

$$\eta_T = 1 - \frac{I_S}{I_{S_0}} \tag{2}$$

where I_{S_0} and I_S represent the emission intensity of Ce^{3+} at the strongest peak (425 nm) in the absence and the presence of Tb^{3+}, respectively. Figure 6c depicts Ce^{3+} and Tb^{3+} relative emission intensities and the values of energy transfer efficiency from Ce^{3+} to Tb^{3+} ions in the $x Tb^{3+}/0.06Ce^{3+}/xLi^{+}$ co-doped wollastonite phosphors. With the increase of Tb^{3+} concentration, the emission intensity of sensitizer Ce^{3+} decreases and intensity of activator Tb^{3+} increases gradually, besides the energy transfer efficiency increases gradually. The maximum value of energy transfer efficiency reaches 62.5% at $x = 0.05$.

The chromaticity coordinates of the $xTb^{3+}/0.06Ce^{3+}/xLi^{+}$ co-doped wollastonite phosphors with Tb^{3+}/Li^{+} content $x = 0.01, 0.03, 0.05, 0.07$ and 0.09 according to the Commission Internationale de L'Eclairage (CIE) are given in Table 2 and Fig. 6d. It is clear that the Ce^{3+}/Li^{+} co-doped sample appears blue and the chromaticity coordinates are located at (0.1384, 0.0567). Following the increasing Tb^{3+} concentration, the colour coordinates change from (0.1384, 0.0567) to (0.2196, 0.2083). Correspondingly, the emitted light also changed from blue to cyan to green. These results show that the obtained samples exhibit the advantages of polychromatic emission in the visible region.

3.5. Temperature dependent luminescence study

The thermal-quenching behaviour of the phosphors is an important issue to be studied, considering the high temperature environment when the LED device is working. Therefore, the thermal stability of the Ce^{3+}/Tb^{3+} doped phosphor is measured. As shown in Fig. 7a, the $0.06Ce^{3+}/0.06Li^{+}$ co-doped wollastonite phosphor exhibits excellent thermal stability. With the temperature increase from 298 to 498 K under 352 nm excitation, the spectral shape and peak position do not change, but the emission intensity decreases slightly. The intensity retains 96.2% of the original value when the temperature is increased to 498 K, which surpasses plenty of reported Ce^{3+}-activated blue phosphors.

In contrast, the $0.12Tb^{3+}/0.12Li^{+}$ co-doped wollastonite phosphor exhibits complex thermal behaviour, as shown in Fig. 7b. With the increase of temperature from 298 to 448 K, the emission intensities of the bands centred at 588 and 620 nm decrease gradually and reach 63.4% and 56.6% of that at 298 K, respectively. Surprisingly, the 545 nm peak exhibits continuous emission enhancement up to 120.3% of that at room temperature when temperature is raised to 448 K, after which it decreases slightly. This intensity enhancement phenomenon caused by the increase of temperature is called thermal anti-quenching performance. One of the widely accepted thermal quenching mechanisms is that excited electrons transition through the intersection between the ground and excited states in the configuration coordinate diagram to ground state via absorbing the thermal energy. Note that the different thermal stability of different emission peaks presently would cause great change in chromaticity coordinate of the $0.12Tb^{3+}/0.12Li^{+}$ co-doped wollastonite phosphor, which seriously restricts the development of the phosphor.

Usually, the intensity of the phosphor will be quenched at high temperature due to the non-radiative transition. The first zero-thermal-quenching $Na_3Sc_2(PO_4)_3:Eu^{2+}$ phosphor and the corresponding mechanism were reported by Kim *et al.* [29]. Thermal anti-quenching of Tb^{3+}-activated green phosphors were also reported previously, such as $Zn_3(BO_3)(PO_4):Mn^{2+},Tb^{3+}$ and $Sr_8ZnSc(PO_4)_7:Tb^{3+}$ [30,31]. In $Zn_3(BO_3)(PO_4):Mn^{2+},Tb^{3+}$ phosphor, the emission intensity of Mn^{2+} and Tb^{3+} all represent zero thermal quenching till the temperature increased to 200 and 150 °C, respectively. As explained, the reason was that shallow defect is induced through rare

Table 2. CIE chromaticity coordinates of $xTb^{3+}/0.06Ce^{3+}/xLi^{+}$ co-doped wollastonite phosphors

Sample	Excitation [nm]	CIE (x,y)
Wo	342	(0.1384, 0.0567)
Wo-Ce/Tb-0.01	342	(0.1809, 0.1035)
Wo-Ce/Tb-0.03	342	(0.1896, 0.1507)
Wo-Ce/Tb-0.05	342	(0.2196, 0.2083)
Wo-Ce/Tb-0.07	342	(0.1964, 0.1348)
Wo-Ce/Tb-0.09	342	(0.1989, 0.1448)

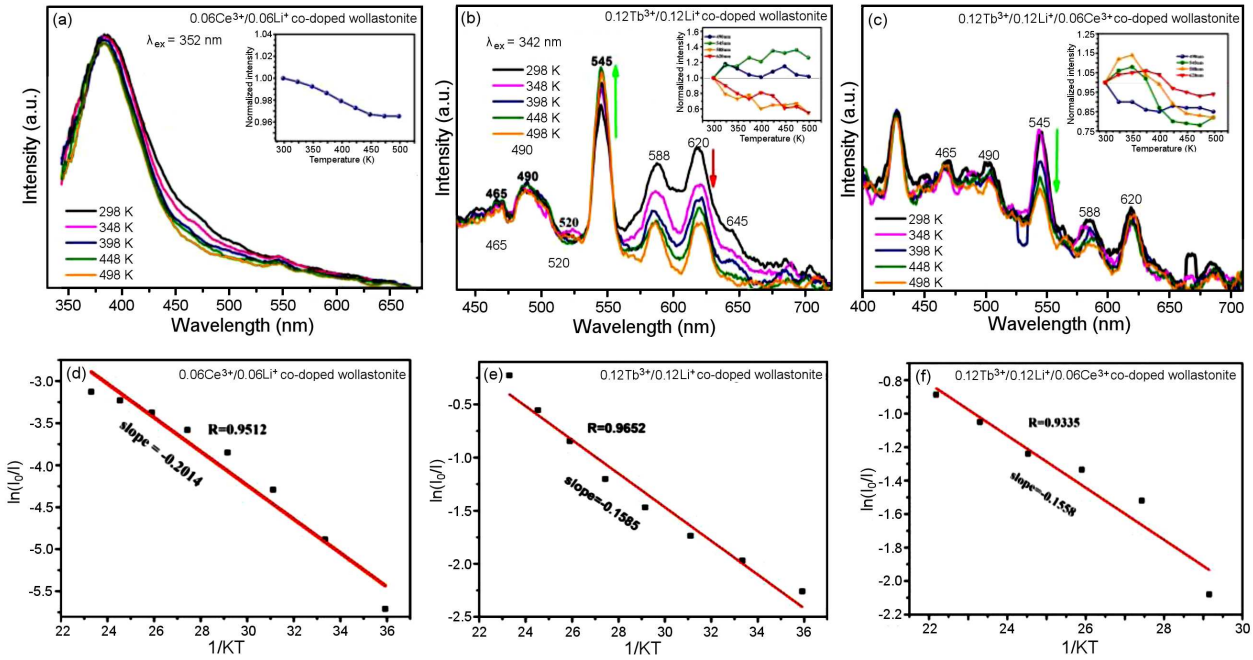

Figure 7. Fluorescence spectra of: a) 0.06Ce^{3+}/0.06Li^+, b) 0.12Tb^{3+}/0.12Li^+ and c) 0.12Tb^{3+}/0.12Li^+/0.06Ce^{3+} co-doped wollastonite phosphors at different temperatures. The Arrhenius ln[(I_0/I) − 1] verses 1/KT plot of: d) 0.06Ce^{3+}/0.06Li^+, e) 0.12Tb^{3+}/0.12Li^+ and f) 0.12Tb^{3+}/0.06Ce^{3+}/0.12Li^+ co-doped wollastonite phosphors

earth ions (Mn^{2+}/Tb^{3+}) doping where the transfer of electron and hole from defect level to activator ions can compensate the emission loss induced by non-radiative transitions, sustaining the emission intensity as temperature increased. For the $Sr_8ZnSc(PO_4)_7$:Tb^{3+} sample, the authors also proposed that defect cluster $Tb_{Zn}^{\bullet}$ + V_{Zn}'' + V_O traps would be generated with different depths, when larger Tb^{3+} ions occupy smaller Zn^{2+} ion sites. Zero-thermal-quenching performances are attributed to the compensation of the emission intensity loss by carriers from various depths at different ambient temperatures. Presently, as compared to synthetic host material, the natural wollastonite induces various intrinsic structural defects, such as point defects, dislocations, grain boundaries, and edges because of impurity ions and metallogenic stress, which can act as different traps and capture electrons and holes. On the other hand, the size mismatch between Tb^{3+}, Li^+ and Ca^{2+} can also generate cation disorder, resulting in the appearance of traps. Under 342 nm excitation, the electrons at the ground state were excited to the $^5L_{10}$ energy level of the Tb^{3+} ion; then, they exhibited non-radiative transition to the $^5D_4$ energy level and subsequently relaxed to the ^7F_J energy levels by generating $^5D_4$-^7F_J green emissions. Some excited electrons could jump into the conduction band with the assistance of thermal disturbances and subsequently were captured by the defect traps. Meanwhile, the captured electrons in different defect trap depths were easily released to the $^5D_4$ energy level of Tb^{3+} at different ambient temperatures, thus compensating for the luminous intensity loss due to their close proximity to each other. The release of electrons from the traps to the $^5D_4$ energy level of Tb^{3+} dominated the compensation of intensity for the luminescence stability at high temperature. The detailed carrier capture and release processes are illustrated in the schematic diagram of the 0.12Tb^{3+}/0.12Li^+ co-doped wollastonite phosphor in Fig. 8.

It is interesting that the co-doping of Ce^{3+} ions changed the thermal behaviour of Tb^{3+} ions. For the 0.12Tb^{3+}/0.06Ce^{3+}/0.12Li^+ co-doped wollastonite phosphor, the thermal loss of the 425 nm blue emission of Ce^{3+} has not changed much compared to the 0.06Ce^{3+}/0.06Li^+ co-doped wollastonite sample. However, the 490 nm emission of Tb^{3+} showed a monotonic decrease, and that of the 545, 588 and 620 nm of Tb^{3+} all exhibited a tendency to increase firstly and then decrease, whose emission intensity at 473 K main-

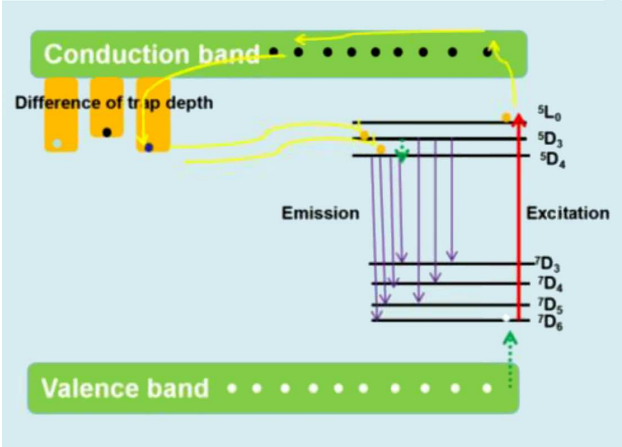

Figure 8. Schematic illustration of the proposed excitation mechanism of Tb^{3+}/Li^+ co-doped wollastonite phosphor

tained 78.3%, 83.5% and 92.6% compared to that at 298 K. Interestingly, not only the energy transfer from Ce^{3+} ions to Tb^{3+} ions did not happen at higher temperature, but also the co-doping of Ce^{3+} ions resulted in a pronounced reduction of Tb^{3+} intensity, compared with the $0.12Tb^{3+}/0.12Li^{+}$ co-doped wollastonite sample. According to the previous study, the thermal stability of Tb^{3+} was usually improved after the incorporation of Ce^{3+} ions, such as $SrMg_{1.06}Al_{9.94}O_{17}:Tb^{3+}$ [24]. Presently, we propose that the introduction of larger Ce^{3+} ions compensates the radius diversity between Tb^{3+}, Li^{+} and Ca^{2+}, thus the number of various defects may be reduced. On the other hand, the reason may be connected to the immediate recombination of the electrons with: i) Ce^{3+} ions and releasing photons, and ii) recombination with trapped holes and releasing phonons. As a result, the number of electrons in the conduction band, which might be captured by different traps decreases causing a strong reduction of thermoluminescence intensity. However, a more in-depth study is still needed in future.

The activation energy (E_a) of thermal quenching process for the samples could be calculated by fitting the thermal quenching data of PL intensity using the following Arrhenius equation [32]:

$$I_T = I_0 \left[1 + C \cdot \exp\left(-\frac{\Delta E}{K \cdot T} \right) \right]^{-1} \qquad (3)$$

where I_0 is the initial fluorescence intensity, I_T is the fluorescence intensity at different temperatures, ΔE is the activation energy of quenching, C is a constant, K is Boltzmann's constant (8.617×10^{-5} eV) and T is temperature. Figures 7d-f show straight lines, obtained by fitting the data presented in Fig. 7a-c. The calculated thermal quenching activation energies of the $0.06Ce^{3+}/0.06Li^{+}$, $0.12Tb^{3+}/0.12Li^{+}$ and $0.12Tb^{3+}/0.06Ce^{3+}/0.12Li^{+}$ co-doped wollastonite phosphors are 0.2014, 0.1585 and 0.1558 eV, respectively. Generally speaking, the higher the value of the activation energy, the better the thermal stability of the phosphor. The results show that the phosphors have good thermal stability and they can be used in high power LED applications.

IV. Conclusions

In this work, $x Tb^{3+}/x Li^{+}$, $y Ce^{3+}/y Li^{+}$ and $x Tb^{3+}/Ce^{3+}/x Li^{+}$ co-doped natural wollastonite phosphors were prepared by high temperature solid state thermal diffusion method at 1150 °C for 2 h in vacuum furnace. Ce^{3+} ions occupy the eight-coordinated Ca^{2+} site and emit intense purple blue light centred at 382 nm, which can be excited both at 284 and 352 nm. Tb^{3+} ions also substitute Ca^{2+} and emit green to yellow light depending on the various doping contents, because of the energy transfer from Tb^{3+} to minor amount of impurity Mn^{2+} existing in the natural wollastonite matrix. Moreover, there is energy transfer from Ce^{3+} to Tb^{3+} in the $x Tb^{3+}/0.06Ce^{3+}/x Li^{+}$ co-doped wollastonite phosphors with Tb^{3+}/Li^{+} content x = 0.01, 0.03, 0.05, 0.07 and 0.09, which can generate a colour-tuneable light. The temperature dependent photoluminescence within the temperature range of 298–498 K demonstrates that the emission intensity of the $0.06Ce^{3+}/0.06Li^{+}$ co-doped wollastonite at 498 K retains 96.2% of that at room temperature. Anti-thermal-quenching phenomenon in the $0.12Tb^{3+}/0.12Li^{+}$ co-doped wollastonite phosphor is observed owning to the traps induced by the doped ions and defect of natural mineral matrix.

Acknowledgements: This work was supported by the Science and Technology project of Hubei Polytechnic University (23xjz02Y), the innovation and entrepreneurship training program for college students of Hubei Polytechnic University (X202310920079), Key Laboratory of Icing and AntiDe-icing of CARDC (Grant No. IADL 20230106) and Natural Science Foundation of Hubei Province (2020CFB496).

References

1. A.G. Bispo-Jr, L.F. Saraiva, S.A.M. Lima, A.M. Pires, M.R. Davolos, "Recent prospects on phosphor-converted LEDs for lighting, displays, phototherapy, and indoor farming", *J. Lumin.*, **237** (2021) 118167.
2. N.U. Islam, M. Usman, S. Rasheed, "White light-emitting diodes: Past, present, and future", *Ecs. J. Solid. State. Sc.*, **10** (2021) 10–16.
3. I. Gupta, S. Singh, S. Bhagwan, D. Singh, "Rare earth (RE) doped phosphors and their emerging applications: A review", *Ceram. Int.*, **47** (2021) 19282–19303.
4. G.B. Nair, H.C. Swart, S.J. Dhoble, "A review on the advancements in phosphor-converted light emitting diodes (pc-LEDs): Phosphor synthesis, device fabrication and characterization", *Prog. Mater. Sci.*, **109** (2020) 100622.
5. A. Krigel, M. Berdugo, E. Picard, R. Levy-Boukris, I. Jaadane, L. Jonet, "Light-induced retinal damage using different light sources, protocols and rat strains reveals LED phototoxicity", *Neuroscience*, **339** (2016) 296–300.
6. Z. Yang, G. Liu, Y. Zhao, Y. Zhou, J. Qiao, M.S. Molokeev, "Competitive site occupation toward improved quantum efficiency of $SrLaScO_4$:Eu red phosphors for warm white LEDs", *Adv. Opt. Mater.*, **10** (2022) 2102373.
7. Z.C. Zhao, Y. Zhou, G.Tan, J. Li, "Research progress about the effect and prevention of blue light on eyes", *Int. J. Ophthalmol.*, **11** [12] (2018) 1999–2003.
8. S.S.B Nasir, A. Tanaka, A. Kato, "Luminescence properties of $Li_2SrSiO_4:Eu^{2+}$ silicate yellow phosphors with high thermal stability for high-power efficiency white LED application", *J. Lumin.*, **207** (2019) 22–28.
9. R. Yantake, A. Sidike, T. Yusufu, "Effect of Eu^{3+} doping on luminescence properties of a $KAlSiO_4:Sm^{3+}$ phosphor", *J. Rare. Earths.*, **40** (2022) 390-397.
10. X.Y. Hu, Z.H. Li, X. Xu, Y.X. Li, "Enhancement of photoluminescence of $Ba_2SiO_4:Eu^{2+}$ by co-doping of La^{3+} or Y^{3+}", *J. Rare. Earths*, **27** (2009) 47–49.
11. Y.L. Zhu, Y.J. Liang, S.Q. Liu, H.R. Li, J.H. Chen, W. Lei, "Design of hierarchical composite silicate for full-color and high thermal stability phosphors", *Chem. Eng. J.*, **345**

(2018) 327–336.
12. T. Yamanaka, H. Mori, "The structure and polytypes of α-$CaSiO_3$ (pseudowollastonite)", *Acta. Crystallogr. B*, **37** (1981) 1010.
13. S.H.M. Poort, H.M. Reijnhoudt, H. Kuip, G. Blasse, "Luminescence of Eu^{2+} in silicate host lattices with alkaline earth ions in a row", *J. Alloys Compd.*, **241** (1996) 75–81.
14. Y.K. Kshetri, B. Chaudhary, D.R. Dhakal, C. Regmi, G. Murali, S.W. Lee, H.T. Kim, "Ultraviolet and visible upconversion in Yb/Er-$CaSiO_3$ β-wollastonite phosphors", *Ceram. Int.,* **49** (2023) 7489–7499.
15. M.X. Ma, D.C. Zhu, Z.X. Wang, T. Han, "Near-ultraviolet excitable pseudo-wollastonite α-$CaSiO_3$:Eu^{2+} blue phosphor for white light-emitting diodes", *Optoelectron. Adv. Mater. Mater. Rapid Commun.*, **17** (2023) 148–151.
16. R.G. Ribas, T.M.B. Campos, V.M. Schatkoski, B.R.C.D. Menezes, T.L.D.A. Montanheiro, G.P. Thim, "α-wollastonite crystallization at low temperature", *Ceram. Int.*, **46** (2020) 6575–6580.
17. N.L. Zhang, J.A. Molenda, S. Mankoci, X.F. Zhou, W.L. Murphy, N. Sahai, "Crystal structures of $CaSiO_3$ polymorphs control growth and osteogenic differentiation of human mesenchymal stem cells on bioceramic surfaces", *Biomater. Sci.*, **1** (2013) 1101–1107.
18. F. Chen, Z.J. Wang, J. Zhang, H. Wang, "Full visible spectra emission of multiple site wollastonite phosphor doped with Eu, La ions", *J. Lumin.*, **226** (2020) 117417.
19. Y.Y. Zhang, H.K. Liu, L.F. Mei, M.S. Molokeev, Y.J. Wang, Z.H. Huang, "Structure and color-tunable luminescence properties of Ce^{3+} and Tb^{3+}-activated $Mg_2La_8(SiO_4)_6O_2$ phosphors based on energy transfer behavior", *J. Solid. State. Chem.*, **255** (2017) 36–40.
20. Q.X. Li, L.Q. Cheng, W.M. Zhang, J.H. Xie, H. Tang, X.Y. Zhang, "Luminescence properties and energy transfer investigations of Ce^{3+} and Tb^{3+} co-doped $NaCaGaSi_2O_7$ phosphors", *Appl. Radiat. Isot.*, **150** (2019) 175–179.
21. Z.Y. Ye, Z.M. Cao, Y.R. Bi, "Luminescence of wollastonite", *Miner. Petrol.*, **10** (1990) 100–104.
22. X.Y. Liu, C.X. Ding, "Phase compositions and microstructure of plasma sprayed wollastonite coating", *Surf. Coat. Technol.*, **141** (2001) 269–273.
23. J.R. Wang, D. Wu, H.B. Duan, H. Liang, Y.P. Wang, J.Q. Peng, X.Y. Ye, "Selective addition of Al^{3+} into Ba_2SiO_4:Eu^{2+} phosphor to improve its luminescence and thermal stability", *ECS J. Solid State Sci. Technol.*, **10** (2021) 066002.
24. J.M. Tang, J.Y. Si, X.Y. Fan, Y.J. Liu, J.H. Li, "Tunable emission, energy transfer and thermal stability of Ce^{3+}, Tb^{3+} co-doped $Na_2BaCa(PO_4)_2$ phosphors", *J. Rare. Earths*, **40** (2022) 878–887.
25. X.G. Zhang, J.L. Zhang, Y.B. Chen, M.L. Gong, "Energy transfer and multicolor tunable emission in single-phase Tb^{3+}, Eu^{3+} co-doped $Sr_3La(PO_4)_3$ phosphors", *Ceram. Int.*, **42** (2016) 13919–13924.
26. Y.H. Jin, Y.H. Hu, L. Chen, X.J. Wang, Z.F. Mu, G.F. Ju, "A novel emitting color tunable phosphor $Ba_3Gd(PO_4)_3$:Ce^{3+}, Tb^{3+} based on energy transfer", *Phys. B Condens. Matter.*, **436** (2014) 105–108.
27. D. Halmurat, T. Yusufu, Q.L. Wang, J.Y. He, A. Sidike, "Rare earth ion Tb^{3+} doped natural sodium feldspar ($NaAlSi_3O_8$) luminescent properties and energy transfer", *Sci. Rep.*, **9** (2019) 14637.
28. H. Chen, Y.H. Wang, "Energy transfer and photo/cathodoluminescence performances investigation of a luminescent material Ce^{3+}/Tb^{3+} co-doped $Na_2Ca_2Si_2O_7$ for multifunctional applications", *J. Alloy. Compd.*, **847** (2020) 156530.
29. Y.H. Kim, V. Arunkumar, B.Y. Kim, S. Unithrattil, E. Kim, S.H. Moon, J.Y. Hyun, K.H. Kim, D. Lee, J.S. Lee, W.B. Im, "A zero-thermal-quenching phosphor", *Nat. Mater.*, **16** (2017) 543–550.
30. S. Liu, Z. Wang, Q. Bao, X. Li, Y. Chen, Z. Wang, L. Guan, Z. Wei, Z. Yang, P. Li, "Abnormal thermal quenching and blue-shift of $Zn_3(BO_3)(PO_4)$: Inducing host defect by doping Mn^{2+} and Tb^{3+}", *Dyes. Pigm.*, **165** (2019) 44–49.
31. Y. Chen, B. Yu, J. Gou, S.F. Liu, "Zero-thermal-quenching and photoluminescence tuning with the assistance of carriers from defect cluster traps", *J. Mater. Chem. C.*, **6** (2018) 10687–10692.
32. G.X. Zhang, J. Zhang, Y.J. Liu, J.Y. Si, X.M. Tao, G.M. Cai, "Structure and luminescence properties of multicolor phosphors with excellent thermal stability based on a new phosphate $Ba_3In_4(PO_4)_6$", *J. Alloys. Compd.*, **797** (2019) 775–785.